Soil Dynamics and Earthquake Engineering 29 (2009) 1236–1248

Contents lists available at ScienceDirect

Soil Dynamics and Earthquake Engineering

journal homepage: www.elsevier.com/locate/soildyn

Efficient 3D nonlinear Winkler model for shallow foundations

H. El Ganainy, M.H. El Naggar *

Department of Civil and Environmental Engineering, University of Western Ontario, London, Ontario, Canada N6A 5B9

ARTICLE INFO

Article history:
Received 1 September 2008
Accepted 18 February 2009

Keywords:
Soil-structure interaction (SSI)
Shallow foundations
Beam-on-a-nonlinear Winkler foundation model (BNWF)
Bounding surfaces
Performance-based design (PBD)

ABSTRACT

This paper presents a new practical modeling approach, based on the beam-on-a-nonlinear Winkler foundation (BNWF) model, to simulate the 3D rocking, vertical and horizontal responses of shallow foundations using structural elements that are readily available in the element library of commercially available structural analysis programs. An assemblage of a moment-rotation hinge, shear hinge connected in series with an elastic frame member attached to the bottom end of ground story columns was proposed to model the response of the footing under combined action of vertical, horizontal and moment loading. To couple the responses of these hinges, two bounding surfaces equations were introduced and derived mathematically: a surface that defines the interaction between the rocking and vertical capacities of the footing along its width and length; and a surface that defines the interaction between the horizontal capacities of the footing along its width and length. Simple calculation steps to evaluate the geometric and mechanical properties of the proposed assemblage of structural elements are provided. The proposed modeling approach was verified using experimental results from large scale model foundations subjected to cyclic loading. Based on this study, it was found that the proposed assemblage can be reliably used in modeling the rocking and horizontal responses of shallow foundations under cyclic loading.

1. Introduction

The performance-based design (PBD) approach requires that soil-foundation-structure interaction (SFSI) analysis becomes an integral part of methods used in seismic evaluation, which can provide safer designs and significant cost savings [3]. In addition, rigid body building failures in recent earthquakes (1985 Michoacan-Guerero, Mexico earthquake—[8], 1999 Kocaeli, Turkey earthquake—[21]) highlighted the importance of incorporating SFSI into seismic designs. This is further corroborated by insights gained from design case studies and earthquake damage distribution studies [12,31].

Shallow isolated footings can be modeled using: the uncoupled approach (uncoupled translational and rotational springs); Winkler approach (distributed vertical and horizontal springs; plasticity-type macro-element formulations using foundation action bounding/yield surfaces; and continuum approaches such as finite element or boundary element methods. The continuum approach is most rigorous, but is computationally intensive and time consuming. The uncoupled approach can model the load-deformation behavior, but cannot predict settlement. The macro-element approach is able to satisfactorily predict the complete foundation response because it accounts for nonlinear behavior and coupling between the responses in all directions. Examples of such models include those by Paolucci [28], Cremer et al. [15], Houlsby and Cassidy [22] and recently Gajan et al. [20]. However, the available macro-element models are based on specified bounding surfaces that may not be applicable to a wide range of problems.

The Winkler model represents a trade-off between the uncoupled and macro-element models. It can simulate progressive mobilization of plastic capacity and the resulting settlement, but the lateral action is uncoupled from the vertical and rotational actions. Housner [23] used the Winkler approach to evaluate the structural response accounting for foundation uplift; and Psycharis and Jennings [29] and Song and Lee [30] used it to examine the effects of rocking and uplift. More recently, Filiatrault et al. [19], Chaallal and Ghlamallah [10], Anderson [7] and Chen and Lai [11] used the Winkler approach to examine the effect of both uplift and yield on structures. These studies demonstrated the ability of the Winkler approach to provide reasonable predictions of the rocking response of various structures.

The development of the Winkler approach into the beam-on-a-nonlinear Winkler foundation (BNWF) approach made it popular among design engineers when modeling SFSI. One of the drawbacks of the BNWF approach is the large number of nonlinear springs that is required to capture the main features of footing behavior and accurately predict its vertical and rocking responses. Hutchinson et al. [24] used 101 vertical springs per footing to model the nonlinear planar response of the shallow

* Corresponding author.
E-mail addresses: helnaggar@eng.uwo.ca, helganai@uwo.ca (M.H. El Naggar).

0267-7261/$ - see front matter © 2009 Elsevier Ltd. All rights reserved.
doi:10.1016/j.soildyn.2009.02.002

foundations of a wall-frame structure. Allotey and El Naggar [2] used 51 vertical nonlinear springs to model the 2D vertical and rocking responses of a shallow foundation. The response analysis of an actual multistory building with several footings would require a large number of nonlinear springs per footing, which would result in a prohibitively large number of degrees of freedom. Consequently, most structural engineers will be tempted to neglect the effect of the foundation on the response of the building by modeling the buildings as fixed at the ground surface.

In this paper, a new modeling approach is introduced for the analysis of the nonlinear response of shallow foundations under lateral cyclic loading in a simplified manner. The approach is intended to facilitate modeling shallow foundations of real multistory buildings at production level. The developed model is based on the BNWF approach, but the foundation is represented in a compact form. The foundation is simulated using an assemblage of three structural elements readily available in the element library of most structural analysis programs, namely: a rotation hinge (or curvature hinge); a shear hinge; and an elastic frame member, connected in series. This assembly is to model the moment-rotation, vertical and shear responses of the foundation in an uncoupled manner. To couple the moment-rotation and vertical responses together, appropriate bounding surfaces were derived mathematically.

2. Proposed modeling approach and components description

Shallow foundations have a finite moment capacity. Consequently, the moment at the bottom of the ground floor columns will be limited to the moment capacity of the supporting footing. In other words, the ground floor columns will act as if they have plastic hinges attached to their bottom end, whose yielding moment is equal to the moment capacity of the supporting footing. Hence, shallow foundations can be conveniently incorporated in structural numerical models as hinges, effectively accounting for soil-structure interaction.

2.1. Moment-rotation hinge and moment-curvature hinge

Most commercial structural analysis software (e.g. SAP2000, ETABS, Perform-3D, etc.) have plastic hinge elements in their element library. These elements have uncoupled moment, torsion, axial force and shear hinges. There are also coupled $P–M_2–M_3$ hinges and coupled $V_2–V_3$ shear hinges, which yield based on the interaction of axial force and bending moments and on the interaction of the biaxial shears at the hinge location, respectively. These hinges simulate material nonlinearity in structural members when conducting a nonlinear static, pushover or nonlinear direct integration time history analyses. Most of these hinges are rigid-plastic hinges (i.e. they resemble rusty hinges that undergo deformation only if the applied force exceeds the ultimate capacity of the hinge without any elastic deformation). The force–deformation relation for such hinges is as shown in Fig. 1, where U represents ultimate condition, L represents strength loss, R represents residual strength and X represents failure condition. Most available hinges can represent strength loss (Fig. 1a), or no strength loss (Fig. 1b).

In BNWF formulations, moment–rotation relations for shallow foundations are generally composed of three segments [4]: a straight segment that corresponds to the initial elastic state; a curved segment corresponding to initial uplift only or initial yield only conditions based on the value of the initial vertical bearing capacity safety factor; and a curved segment corresponding to uplift and yield condition.

To model this moment–rotation relation in computationally efficient manner, an idealized relation using straight lines should be used. As recommended by FEMA 356 [6] document, this relation can be idealized as a bilinear relation (or an elastic-perfectly plastic (E-P-P) relation). The slope of the elastic segment in the bilinear relation is equal to the initial slope of the actual moment–rotation relation, and its ultimate moment capacity is equal to the ultimate moment capacity of the actual moment–rotation relation, as shown in Fig. 2.

Accordingly, available hinges in structural analysis codes cannot be used to simulate the moment-rotation behavior of shallow foundations as they cannot accommodate the elastic segment of the footing moment-rotation behavior. To overcome this problem, an elastic frame member should be connected in series with the moment-rotation hinge, as shown in Fig. 3, so that the overall moment–rotation relation for this assembly is a bilinear (or elastic-perfectly plastic (E-P-P)) relation. The length (L_T) and curvature stiffness (EI) of this elastic member should be

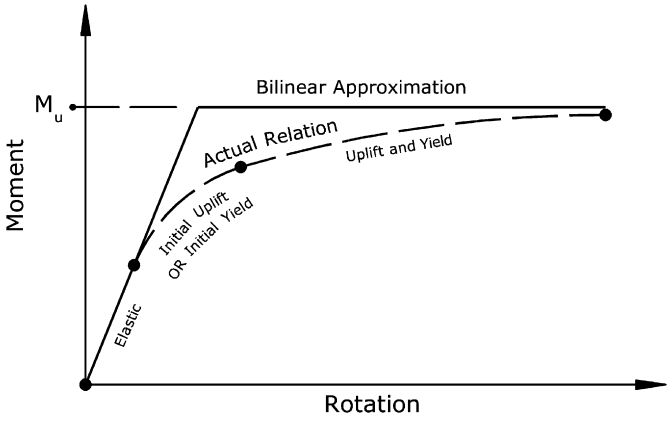

Fig. 2. Actual moment–rotation relation for shallow foundations and proposed bilinear approximation.

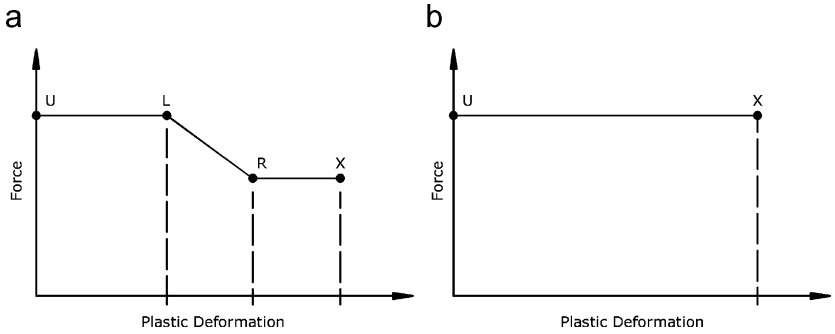

Fig. 1. Force–deformation relation for rigid-plastic hinges: (a) strength loss enabled; (b) strength loss disabled.

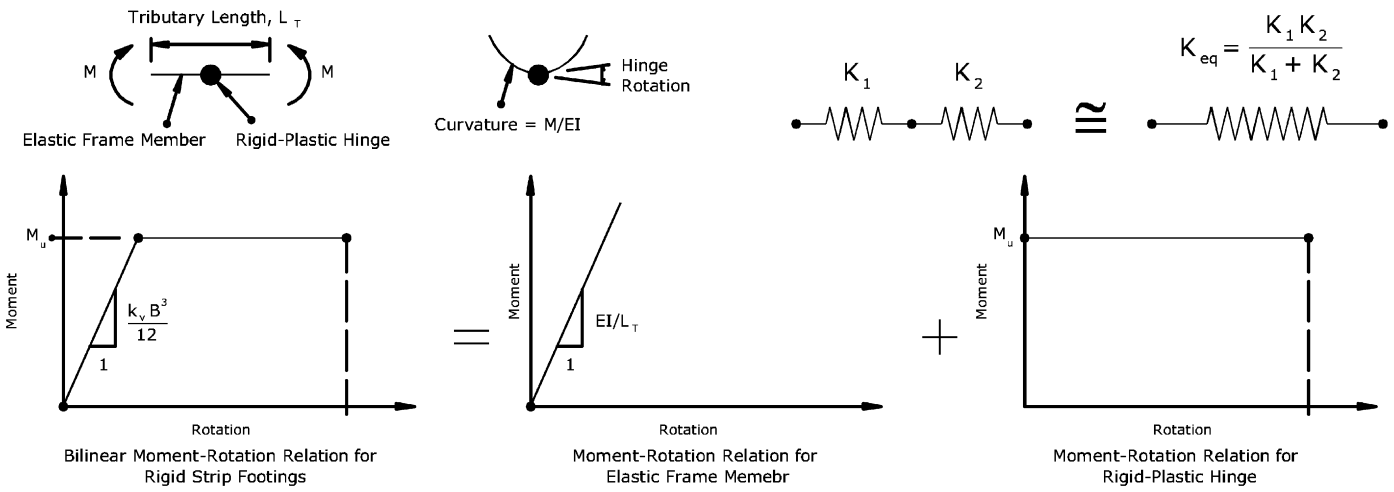

Fig. 3. Assemblage proposed to model shallow strip foundations' moment-rotation behavior.

calculated to give the desired initial slope for the bilinear moment–rotation relation. The calculations will involve three tributary independent parameters; length (L_T), modulus of elasticity (E) and moment of inertia (I) of the elastic member, and only the following equation to be satisfied (with reference to Fig. 3):

$$\frac{EI}{L_T} = \frac{k_v B^3}{12} \tag{1}$$

Two of these parameters should be reasonably assumed to calculate the third. It should be noted from Fig. 3 that using an elastic frame member to give the required elastic rotational stiffness is based on the assumption that the curvature of the elastic member is constant along its length. This assumption is valid only for frame members of infinitesimal lengths. Thus, the minimum possible length allowed by the program should be used. The choice of appropriate values for the modulus of elasticity (E) and moment of inertia (I) to satisfy Eq. (1) will be governed by the required vertical stiffness of the foundation, as will be shown later.

Eq. (1) is derived assuming a unit width for the footing (strip footing). El Ganainy [16] has extended the moment–rotation curve equations given by Allotey and El Naggar [4] for strip footings to the case of rectangular footings. Eqs. (2) and (3) give the bilinear approximation of the moment–rotation relation for rectangular footings in terms of the footing width (B) and length (L), as shown in Fig. 2 [16].

Slope of Elastic Segment:

$$M = \frac{k_v B^3 L\theta}{12} \rightarrow \text{Linear relationship} \tag{2}$$

Ultimate Moment Capacity:

$$M_u = \frac{PB}{2} - \frac{P^2}{2q_u L} \tag{3}$$

where P is the applied vertical load, (F); M is the applied moment along footing width, ($F.L$); θ is the footing rotation along its width, (Radians); k_v is the subgrade modulus of the foundation soil, (F/L^3); q_u is the ultimate bearing capacity of the foundation soil, (F/L^2); B is the footing width, (L); L is the footing length, (L).

Considering Eq. (2), Eq. (1) can be rewritten for the case of rigid rectangular footings, i.e.

$$\frac{EI}{L_T} = \frac{k_v B^3 L}{12} \tag{4}$$

which should be satisfied when choosing the length (L_T) modulus of elasticity (E) and moment of inertia (I) of the elastic member for the proposed assembly. Similar to the case of strip footings, L_T should be minimal and E and I should be selected with due consideration of the vertical stiffness.

Some structural analysis programs (e.g. Perform-3D) have curvature hinges in their element library. Curvature hinges are essentially the same as rotation hinges, but they use a moment–curvature relationship rather than moment-rotation to define the action–deformation relationship for the hinge. This facilitates modeling plastic zones in structural members, especially when interpreting experimental results [13,14]. Fig. 4 shows the concept for a curvature hinge.

A curvature hinge requires a moment–curvature relationship and a tributary hinge length. This is typically modeled in available computer programs using a rigid-plastic rotation hinge and an elastic frame member. The tributary length is used to convert the moment–curvature relationship to an equivalent moment–rotation relationship. The rigid-plastic rotation hinge accounts for the rigid-plastic rotation while the elastic frame segment adjacent to the hinge accounts for the elastic curvature experienced by the plastic zone prior to yielding, as shown in Fig. 5.

Curvature hinges can be readily adapted to model the moment–rotation relation for shallow foundations. The parameters that need to be defined in this case are the moment–curvature relation for the hinge and the hinge length. With the hinge length (L_T) taken as the minimum possible length allowed by the program, the moment–curvature relation for the hinge can be calculated from the specified moment–rotation relation for the footing. Knowing the rotation ordinate and the selected hinge length, the curvature ordinate can be calculated, i.e.

$$\psi = \frac{\theta}{L_T} \tag{5}$$

where (ψ) is the curvature and (θ) is the rotation of the hinge.

2.2. P–M_B–M_L bounding surface

The seismic response of buildings involves two forms of rocking; local rocking of individual footings and global rocking of the whole building. The proposed approach for modeling local rocking was discussed in the previous section. Global rocking can have a significant effect on the structural response, especially for slender buildings where the response is mainly governed by the overall bending effect. Global rocking varies the vertical loads

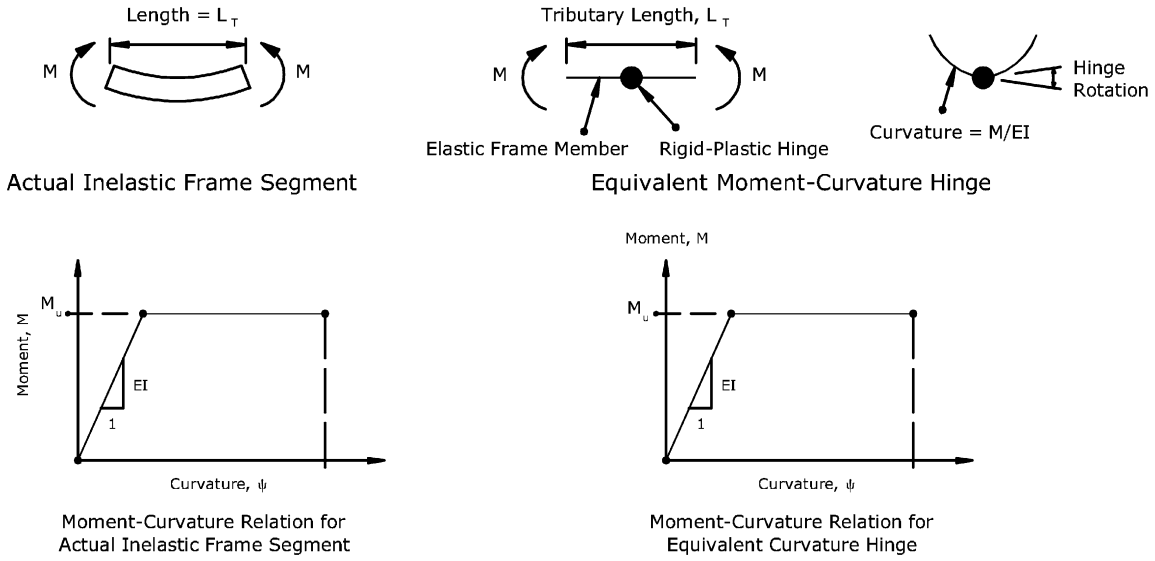

Fig. 4. Concept of curvature hinge.

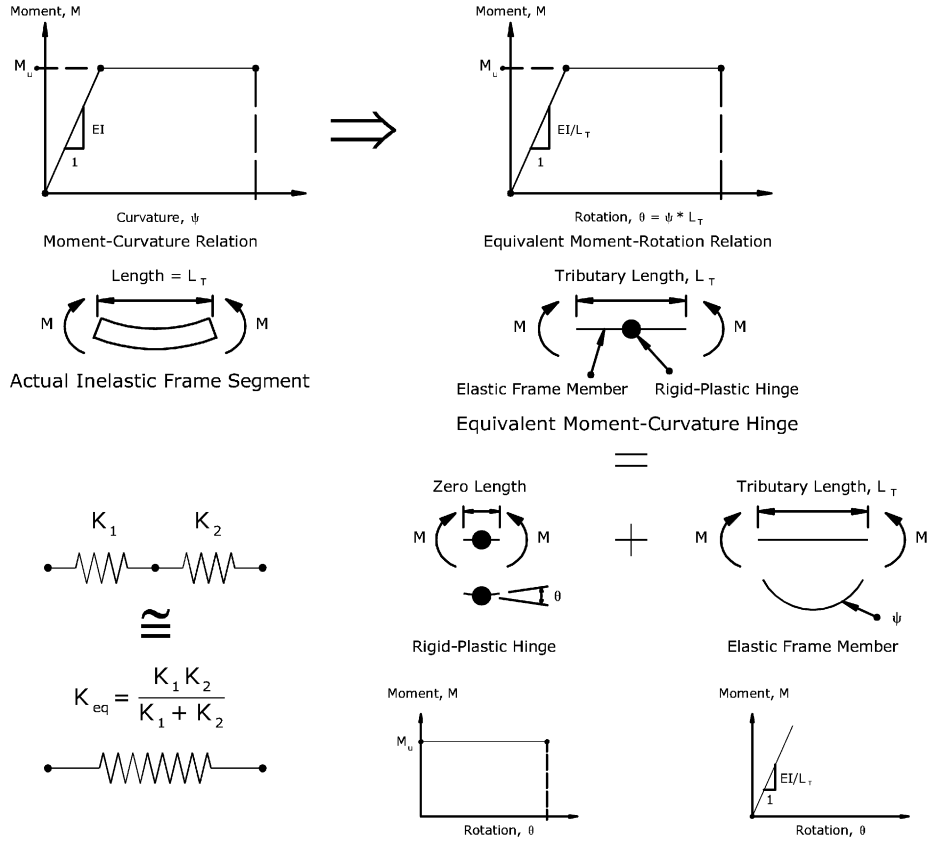

Fig. 5. Modeling curvature hinges.

acting on individual foundations. This variation could alter the moment capacity of these footings due to the interaction between the vertical load and the moment capacity of the footing.

Allotey and El Naggar [4] showed that, based on the BNWF model, for uniform stiffness and bearing capacity distributions, the moment capacity of a rigid strip footing varies in a parabolic manner with the inverse of its vertical bearing capacity safety factor, χ. Fig. 6 shows a similar relationship derived for the case of a rectangular footing of width (B) and length (L), and presented in terms the vertical load, P, and the moment capacity of the footing, M_u.

The BNWF approach implicitly accounts for the interaction between the applied vertical load and the footing moment capacity. On the other hand, the moment-rotation hinge approach can account for this interaction only if it was explicitly simulated using an appropriate bounding surface.

To define the complete bounding surface that relates the vertical load (P) to the moment capacity of the footing (M_u) along

its width (B) and length (L), two relations should be defined: interaction between (P) and (M_u) in case of uniaxial moment loading; and interaction between the moment capacities of the footing along its width (B) and length (L) in case of biaxial moment loading.

Decoupling the effect of horizontal loads at this stage, Fig. 6 can be used to define the bounding surface that represents the interaction between (P) and (M_u). Allotey and El Naggar [4] have shown that for a strip footing, regardless of the value of the vertical bearing capacity safety factor, the last curved segment of its moment–rotation curve that corresponds to the uplift and yield condition can be represented as follows:

$$M = \frac{q_u B^2}{2}(\chi - \chi^2) - \frac{q_u^3}{24 k_v^2 \theta^2} \tag{6}$$

Rewriting Eq. (6) for rectangular footings in terms of (B) and (L), and by considering its limit as $\theta \to \infty$, yields

$$M_u = \lim_{\theta \to \infty} M = \frac{q_u B^2 L}{2}(\chi - \chi^2) \tag{7}$$

Substituting the value of $\chi = P/(q_u BL)$ and rearranging, the bounding surface is obtained, i.e.

$$M_u = \frac{B}{2}\left(P - \frac{P^2}{q_u BL}\right) \tag{8}$$

Making use of similarity in shape between the convex moment capacity–vertical load relation for rectangular footings given by Fig. 6, and the convex bounding surface proposed by El-Tawil and Deierlein [17,18] for inelastic beam-column elements, the bounding surface for rectangular footings is derived and is presented in Fig. 7. Considering the symmetry of the bounding surface and the fact that footings do not possess tension capacity, the bounding surface equations proposed by El-Tawil and Deierlein [17,18] can be rewritten for rectangular footings in more compact form, i.e. (as depicted in Fig. 8)

$$\left(\frac{M_B}{M_{Bn,p}}\right)^n + \left(\frac{M_L}{M_{Ln,p}}\right)^n = 1.0 \tag{9}$$

$$\frac{M_{Bn,p}}{M_{Bnb}} = \left(1 - \left(\frac{|P - P_{bn}|}{P_n - P_{bn}}\right)^m\right) \tag{10}$$

$$\frac{M_{Ln,p}}{M_{Lnb}} = \left(1 - \left(\frac{|P - P_{bn}|}{P_n - P_{bn}}\right)^m\right) \tag{11}$$

where M_B, M_L is the moment capacities pairs of the footing along its width, B, and length, L, respectively, in case of biaxial moment loading; $M_{Bn,p}$ is the moment capacity of the footing along its width, B, under vertical load P; $M_{Ln,p}$ is the moment capacity of the footing along its length, L, under vertical load P; M_{Bnb} is the moment capacity of the footing along its width, B, at the balanced point; M_{Lnb} is the moment capacity of the footing along its length, L, at the balanced point; P is the current vertical load; P_{bn} is the vertical load at the balanced point; P_n is the vertical load capacity of the footing; n is the fitting exponent that controls the shape of the bounding surface in (M_{Bn}–M_{Ln}) plane; m is the fitting exponent that controls the shape of the bounding surface in (P–M_{Bn}) and (P–M_{Ln}) planes.

To define the interaction surface between (P) and (M_u) in case of uniaxial moment loading, Eq. (8) is used together with Eq. (10) (or Eq. (11)). Substituting values of $M_{Bn,p}$, M_{Bnb}, P_{bn} and P_n in Eq. (10) yields

$$\frac{M_u}{\left(q_u B^2 L/8\right)} = \left(1 - \left(\frac{|P - (q_u BL/2)|}{q_u BL - (q_u BL/2)}\right)^m\right) \tag{12}$$

Substituting the value of M_u from Eq. (8) into Eq. (12) yields

$$\frac{B/2(P - P^2/q_u BL)}{(q_u B^2 L/8)} = \left(1 - \left(\frac{|P - (q_u BL/2)|}{q_u BL - (q_u BL/2)}\right)^m\right) \tag{13}$$

Simplifying Eq. (13) and substituting $I = (2P/q_u BL)$ yields

$$2I - I^2 = (1 - (I-1)^m) \tag{14}$$

Solving Eq. (14) gives $m = 2$. Thus, the bounding surface for a rectangular footing that describes interaction between (P) and (M_u) along its width, B, in case of uniaxial moment loading and based on the BNWF model with uniform stiffness and bearing capacity distributions, can be expressed as

$$\frac{M_u}{(q_u B^2 L/8)} + \left(\frac{P - (q_u BL/2)}{q_u BL/2}\right)^2 = 1 \tag{15}$$

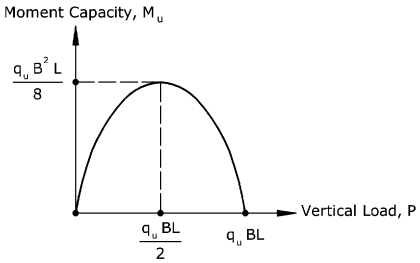

Fig. 6. Variation of moment capacity of rectangular footings with applied vertical load.

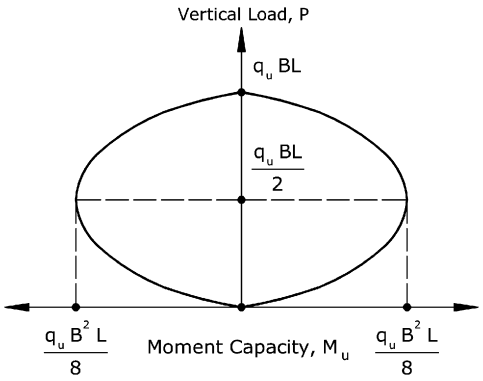

Fig. 7. Variation of moment capacity of rectangular footings with applied vertical load considering positive and negative footing moment capacity.

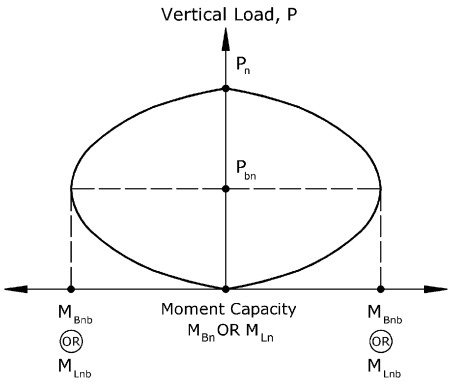

Fig. 8. P–M_u bounding surface of rectangular footings.

To define the interaction surface between the moment capacities of the footing along (B) and (L) in case of biaxial moment loading, another approach is adopted rather than mathematical derivation due to the challenges in defining such 3D relation mathematically using the BNWF approach. Eq. (9) which defines this relation will be calibrated numerically to obtain the fitting exponent (n) which controls the shape of this relation.

El-Tawil and Deierlein [17,18] stated that the strength parameters (i.e. axial and moment capacities) in the bounding surface equations depend on the geometric and mechanical properties of the cross-section under consideration. Thus, they must be calculated for every cross-section. However, the fitting exponent of the surface that controls its shape need only to be determined by calibration to representative cross-sections and do not need to be calculated for each case. Due to the similarity between the rotational behavior of shallow footings and cross-section of structural members, the fitting exponent needs to be determined for the case of shallow foundations once for representative footings plan geometry as well.

The behavior of a shallow footing can be represented using an inelastic frame element formulated based on the fiber cross-section approach. In this approach, the cross-section is discretized into independent fibers that can be of different materials. Each material type is defined by its uniaxial stress–strain relationship, whereas the axial load and biaxial moments acting on the cross-section are applied at its centerline (which implies that plane sections remain plane after deformation). The axial stress in each fiber is calculated using the stress–strain relationship for this fiber and its compression or extension.

From a geotechnical prospective, the fiber section approach is similar to the BNWF approach as it can be seen as modeling cross-sections using closely spaced discrete independent springs, each has a nonlinear force–deformation relationship. Hence, an inelastic frame element with a fiber cross-section can simulate the behavior of a shallow foundation if the soil properties are assigned to the fibers material, and the area properties (i.e. area and moment of inertia about both axes) of the fiber section as a whole are equal to the area properties of the modeled footing. The fiber cross-section approach is readily available and coded in many structural analysis codes (e.g. Perform-3D, SeismoStruct, ZeusNL). In the current study, Perform-3D [13,14] is used.

Eq. (9) is calibrated to establish the exponent (n) that fits the bounding surface for a shallow foundation employing a model that comprises one inelastic frame element fixed at its base. A fiber cross-section comprising 49 inelastic fibers is assigned to this element. Since the fitting exponent, n, of the surface depends only on the geometric properties of the cross-section under consideration and does not depend on the mechanical properties of the section [17,18], the calibration will be performed for rectangular footings of different aspect ratios (L/B): 1.0, 2.0, 4.0 and 6.0. The bounding surfaces for these aspect ratios are calibrated at the balanced point where vertical bearing capacity safety factor ($1/\chi$) is equal to 2.0 ($\chi = 0.50$).

To examine the shape of the bounding surface under different values of χ, the case of square footing was analyzed for $\chi = 0.67$ and 0.33. These values are equidistant from the balanced point on both sides. To reduce the number of variables involved in the analysis, only one soil type was considered. The soil was assumed to be dense sand of ultimate bearing capacity, $q_u = 1500\,\text{kN/m}^2$, subgrade modulus, $k_v = 280{,}000\,\text{kN/m}^3$. The width of the footing was taken as 0.7 m and the footing length was calculated to give the desired aspect ratio. The width of the fibers was 0.1 m and its length is calculated according to the footing length. The parameters that define each fiber are: its area, location within the section, and the uniaxial stress–strain relationship.

The soil is idealized as an elastic-perfectly plastic material, where the ultimate strength of the fibers is equal to the ultimate bearing capacity of the soil, q_u, and the slope of the elastic branch is equal to the modulus of elasticity of the foundation soil, which can be calculated from the axial stiffness of the fibers and the subgrade modulus of the soil as follows:

$$\frac{EA_F}{L_T} = k_v A_F \tag{16}$$

where E is the equivalent modulus of elasticity for foundation soil, (kN/m^2); k_v is the subgrade modulus of foundation soil, (kN/m^3); A_F is the area of the whole footing or area of individual fibers, (m^2); L_T is the length of the frame member, (m).

The length, L_T, of the frame member considered is 0.20 m.

The bounding surface calibration involved two steps. Eq. (3) is used to calculate the footing ultimate moment capacity along width, $M_{u,B}$, and length, $M_{u,L}$ (for calculating $M_{u,L}$, the values of B and L are interchanged in Eq. (3)). The moment capacities are compared with the moment capacities calculated numerically by Perform-3D. The numerical analysis involved applying a concentrated moment at the top of the frame element that represents the Winkler foundation. The value of this moment is taken larger than the moment capacity calculated using Eq. (3). This moment is applied in small increments increasing monotonically. The moment capacity of the footing is established from the resulting moment–curvature curve, and is given by the ultimate moment capacity of the curve. Table 1 summarizes the different cases analyzed and compares the numerical and the analytical results.

The interaction between footing moment capacities along its width and length, in case of biaxial moment loading is then investigated. This is achieved by applying a moment increasing incrementally from zero to 100% of $M_{u,L}$ while maintaining a moment equal to 10% of $M_{u,B}$ along its width. The reduced moment capacity is obtained from the resulting moment–curvature curve for the footing along its length. This scenario is repeated, with 20%, 30%, …, 100% of $M_{u,B}$ applied along the width of the footing. It should be noted that reversing footing width and

Table 1
Different scenarios assumed in analysis series and corresponding results from the numerical analysis and analytical equation.

Case number	Vertical bearing capacity safety factor ($1/\chi$)	L/B	B (m)	L (m)	$M_{u,B}$ (kN m)		$M_{u,L}$ (kN m)	
					Numerical analysis	Analytical equation	Numerical analysis	Analytical equation
1	2.0	1.0	0.70	0.70	63.36	64.31	63.36	64.31
2	1.5	1.0	0.70	0.70	56.31	57.17	56.31	57.17
3	3.0	1.0	0.70	0.70	56.46	57.17	56.46	57.17
4	2.0	2.0	0.70	1.40	126.73	128.63	253.45	257.25
5	2.0	4.0	0.70	2.80	253.45	257.25	1014.20	1029.00
6	2.0	6.0	0.70	4.20	380.18	385.88	2283.80	2315.25

length in these analyses yielded the same pairs for moment capacities.

Eq. (9) is calibrated against these results by plotting the moment capacities pairs obtained from the numerical analyses and those given by the equation. The fitting exponent, n, is adjusted to yield the best match. As shown in Fig. 9, Eq. (9) with $n = 1.8$ provides excellent prediction for the normalized moment (normalized by the corresponding moment capacity of the footing along its width and length).

Thus, the bounding surface for rectangular footings that describes the interaction between the moment capacities of the footing along its width, M_B, and length, M_L, in case of biaxial moment loading for BNWF model with uniform stiffness and bearing capacity distributions, can be expressed as

$$\left(\frac{M_B}{M_{Bn,p}}\right)^{1.8} + \left(\frac{M_L}{M_{Ln,p}}\right)^{1.8} = 1.0 \tag{17}$$

Using Eqs. (15) and (17), the complete $P–M_B–M_L$ bounding surface for rectangular footings can be defined, assuming uniform stiffness and bearing capacity distributions. Fig. 10 shows a schematic of the normalized bounding surface drawn in $P–M_B–M_L$ space.

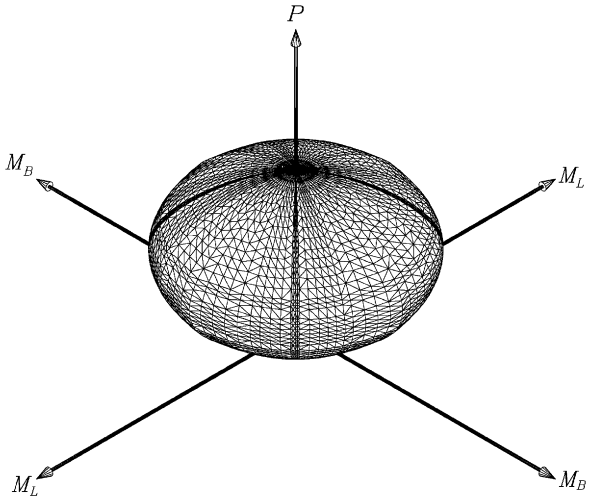

Fig. 10. Schematic of normalized $P–M_B–M_L$ bounding surface for rectangular footings.

2.3. $V_B–V_L$ shear hinge

Under seismic excitations, building foundations experience horizontal inertia forces transmitted from the superstructure to the foundation soil (i.e. base shear). If base shear exceeds the ultimate horizontal capacity of the foundation, it undergoes hysteretic force-deformation action providing an additional source for dissipating the earthquake energy.

For shallow foundations subjected to horizontal and vertical loading, there are two possible failure modes: bearing capacity failure in the foundation soil by the formation of a slip surface; or failure in the footing-soil interface by sliding. The bearing capacity failure may result from the resultant inclined load acting on the footing. If the horizontal load is increased gradually up to failure, the formed slip surface will be shallow, skewed in the direction of load application and will occur on that side only (Fig. 11).

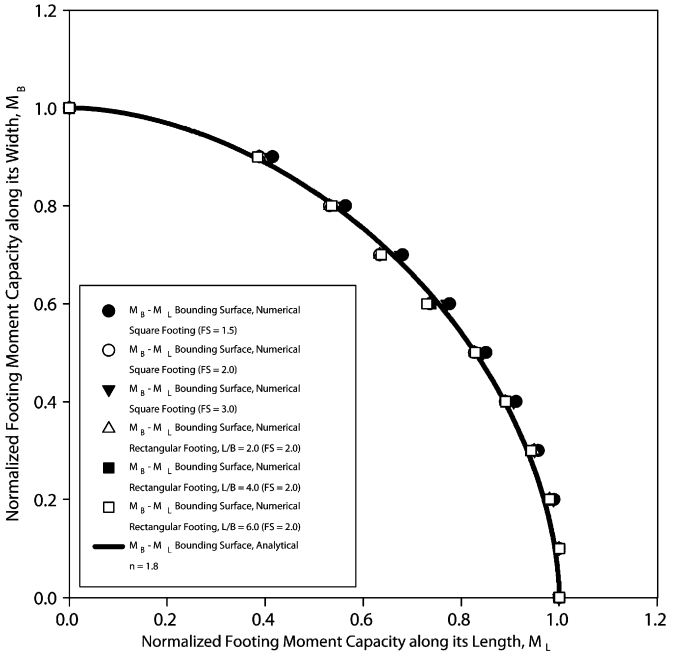

Fig. 9. Normalized $M_B–M_L$ bounding surface for rectangular footings.

The footing experiences a reversal in the direction of seismic horizontal load. The formation of the failure mechanism shown in Fig. 11 requires a sustained horizontal loading, thus rendering this failure mechanism less probable to occur. The bearing capacity failure, if occurred, will most likely be due to vertical loading. The other failure mechanism involves sliding at the footing–soil interface. This failure mechanism is presented in most building codes and seismic provisions (e.g. [5,6,9]).

The footing horizontal capacity, F_u, considering sliding at the footing–soil interface arises from three components (Fig. 12): base friction, R_1, which is the main resistance mechanism that contributes to the footing horizontal capacity; soil passive resistance, R_2, along the front face of the footing; and side friction, R_3, resulting from friction at the footing side–soil interface. FEMA 356 [6] document provides guidelines for calculating the footing horizontal capacity components and presumptive values depending on the type of foundation soil.

Shear hinges attached to the bottom of ground floor columns are used herein to model the horizontal force-displacement response of the supporting footings. These shear hinges account for the elastic horizontal stiffness of the foundation soil, its horizontal capacity and the inelastic energy dissipated in the hysteresis force-deformation action under cyclic loading. In the case of biaxial horizontal loading, an appropriate bounding surface is used to account for the interaction between the footing horizontal capacities along its width and length.

To account for elastic force-deformation action, an elastic frame member is connected in series with the shear hinge, as shown in Fig. 13. The length (L_T) and shear area (A_S) of this elastic member should be calculated to give the desired initial slope for the horizontal force–deformation relation of the foundation that represents the elastic horizontal stiffness of the foundation soil, K_H (F/L).

The calculations involve three tributary independent parameters: length (L_T); shear modulus (G); and shear area (A_S) of the elastic member, but one equation is to be satisfied (see Fig. 13), i.e.

$$\frac{GA_S}{L_T} = K_H \tag{18}$$

Hence, reasonable values should be assumed for two parameters and the third parameter is calculated accordingly.

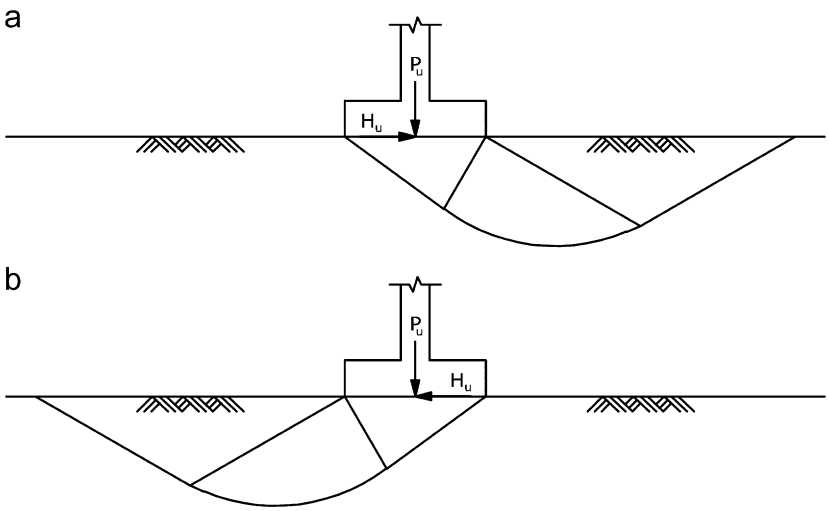

Fig. 11. Schematic of bearing capacity failure surface for shallow foundations in case of horizontal and vertical loading: (a) horizontal load acting to the right; (b) horizontal load acting to the left.

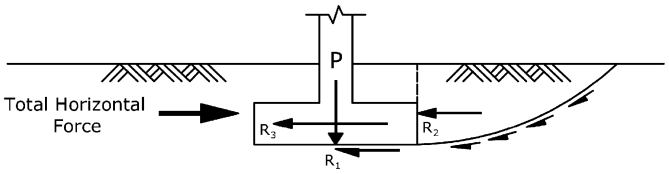

Fig. 12. Footing horizontal capacity components considering failure at footing-soil-interface by sliding.

A moment-rotation hinge and a shear hinge are attached together at the bottom end of each ground story column to fully describe the behavior of shallow foundations accounting for the moment-rotation and horizontal response, respectively. Since both hinges comprise a rigid-plastic hinge and an elastic frame member connected in series, it is possible to use only one elastic frame member connected in series with the two rigid-plastic hinges as shown in Fig. 14. However, the properties of the elastic frame member shared by the two hinges should be calculated to give the desired parameters for each deformation mode.

The frame member properties (L_T, A, A_S, I, E and G) should satisfy the following equations:

$$\frac{EI_B}{L_T} = \frac{k_v B^3 L}{12} \text{ (Rocking along } B\text{)}$$
$$\frac{EI_L}{L_T} = \frac{k_v L^3 B}{12} \text{ (Rocking along } L\text{)} \quad (19)$$

$$\frac{EA}{L_T} = k_v A_F \quad (20)$$

$$\frac{GA_{S(B)}}{L_T} = K_{H(B)} \text{ (Translating along } B\text{)}$$
$$\frac{GA_{S(L)}}{L_T} = K_{H(L)} \text{ (Translating along } L\text{)} \quad (21)$$

$$G = \frac{E}{2(1+v)} \quad (22)$$

To choose a consistent set of member parameters, assuming that the stiffness values k_v and K_H are known, the following procedure is followed:

(1) The minimum possible length (L_T) for elastic frame members is used to ensure constant curvature along the length and to minimize the elastic shear deformations resulting from bending action (i.e. to model racking behavior only).
(2) Knowing L_T, the ratio I/A (where I and A are the member's moment of inertia and cross-sectional area) can be calculated by solving Eqs. (19) and (20) simultaneously. An appropriate value for A is assumed, say 1.0, and the corresponding moments of inertia (I_B) and (I_L) for rocking along the footing width, B, and length, L, are calculated.
(3) Given I_B, I_L and A, the corresponding modulus of elasticity (E) is calculated using either Eqs. (19) or (20) and then (G) is calculated from Eq. (22), assuming an appropriate value for Poisson ratio (v), say 0.3. The shear areas ($A_{S(B)}$) and ($A_{S(L)}$) for shear deformation along B and L are then calculated considering Eq. (21).

To model the interaction between the footing horizontal load capacity along B and L, an appropriate bounding surface is defined for the shear hinge. The horizontal load capacity, F_u, is derived primarily from the shearing resistance at the footing base–soil interface. Assuming uniform bearing pressure on the foundation soil, this shearing resistance, and hence the horizontal capacity, does not depend on the direction of the resultant horizontal load acting on the footing. This is expressed graphically in Fig. 15. For a square footing subjected to biaxial loading conditions, the bounding surface for the footing horizontal capacity can be represented by a circle with radius equal to the footing horizontal capacity, as shown in Fig. 15. On the other hand, rectangular footings will have different capacity along B and L. Consequently, the bounding surface becomes an ellipse, where the minor and major radii are equal to the footing horizontal capacity along B and L, respectively.

The equation for the bounding surface of the footing horizontal capacity in case of biaxial horizontal loading can therefore be described using an elliptical equation, i.e.

$$\left(\frac{V_B}{V_{Bn}}\right)^2 + \left(\frac{V_L}{V_{Ln}}\right)^2 = 1.0 \quad (23)$$

where V_B,V_L is the horizontal load capacity pairs of the footing along B and L, for biaxial loading; V_{Bn} is the horizontal load capacity along B for uniaxial horizontal loading (calculated assuming a constant vertical load); V_{Ln} is the horizontal load capacity along L for uniaxial horizontal loading (calculated assuming a constant vertical load).

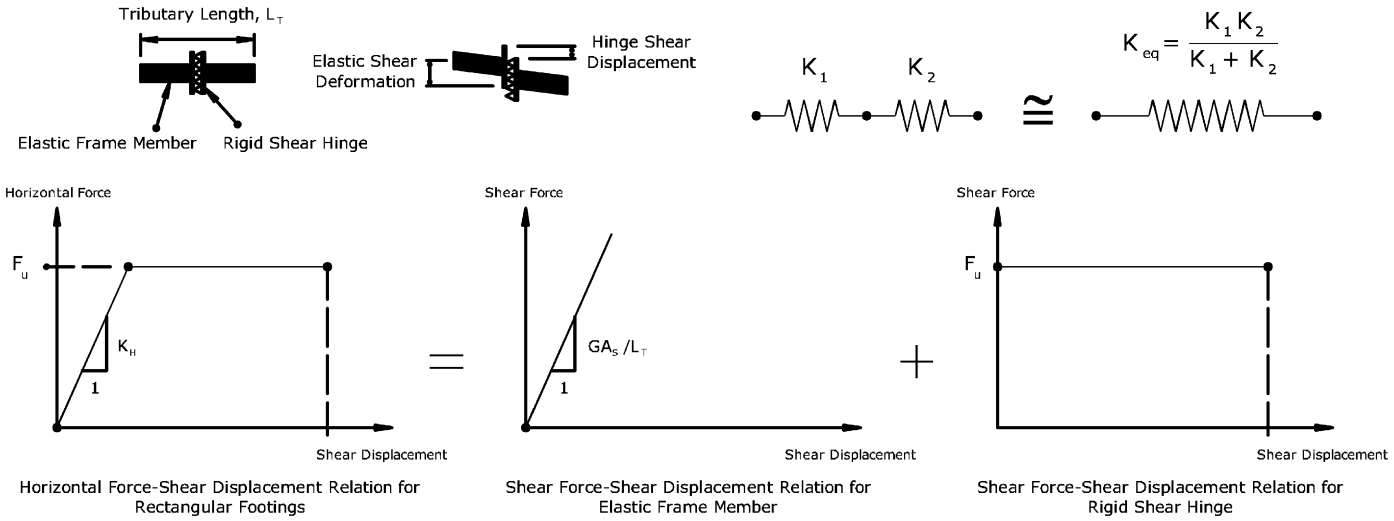

Fig. 13. Assemblage proposed to model rectangular footings' horizontal force-deformation behavior.

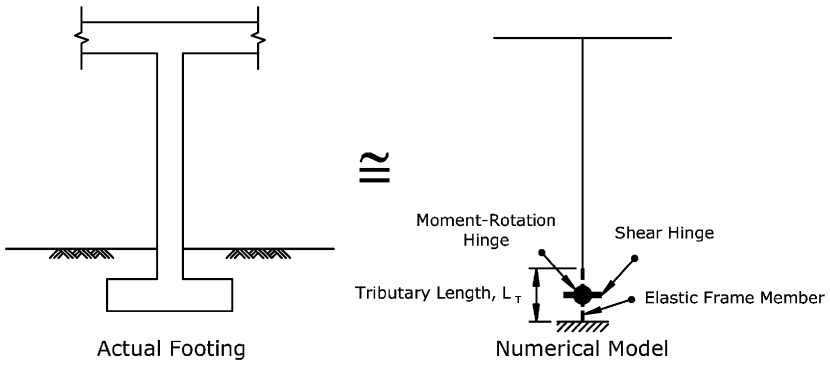

Fig. 14. Proposed numerical model for simulating the behavior of shallow foundations.

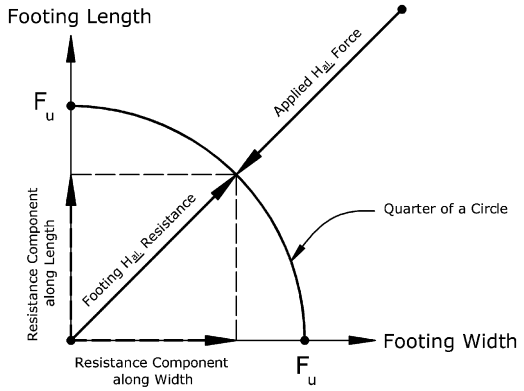

Fig. 15. Graphical representation of square footings horizontal capacity components along its width and length.

3. Comparison with experimental results

To verify the ability of the proposed simplified modeling approach to predict the important aspects of shallow foundations' response under monotonic and cyclic vertical, horizontal and moment loading actions, its predictions are compared with available experimental results. Currently, there are no available experimental investigations for the interaction between the moment capacities and horizontal capacities under biaxial conditions. Therefore, the verification of the proposed modeling approach is limited to 2D loading conditions.

The proposed assembly of a moment-rotation hinge is used to study the moment-rotation behavior and horizontal force-deformation response of a model rigid shallow foundation subjected to a cyclic rocking action. The European Commission (EC) sponsored the project TRISEE (3D Site Effects of Soil-Foundation Interaction in Earthquake and Vibration Risk Evaluation), which included large-scale 1 g model testing to examine the response of rigid footings to dynamic loads. The results of these tests are of high quality and are readily available ([27]). The results from this study are used for validating the proposed modeling approach. The nonlinear structural analysis program Perform-3D [13,14] is used in this study. The calculated moment-rotation and horizontal force-deformation hysteresis loops are compared with the measured results.

3.1. TRISEE large-scale 1 g experiment

The TRISEE experiment was carried out at the European Laboratory for Structural Assessment (ELSA) in Ispra, Italy. The foundation was a 1 m square steel plate with a concrete interface placed on a saturated layer of Ticino sand. The sand was contained in a stiff concrete caisson with dimensions $4.6\,m \times 4.6\,m \times 3\,m$. The caisson's depth minimized the interface of caisson's bottom

with any failure mechanism. The lateral boundaries on the other hand, were relatively close to the foundation and most likely influenced the response of the system [4].

Ticino sand is uniform coarse-to-medium silica sand with $D_{50} = 0.55$ mm, coefficient of uniformity, $C_u = 1.6$, specific gravity, $G_s = 2.684$, $e_{min} = 0.579$, $e_{max} = 0.931$ and constant volume frictional angle, $\phi'_{cv} = 35^\circ$ [27]. The footing was embedded 1 m below soil surface, with a steel formwork placed around the footing to retain the soil (i.e. the sides were not in contact with soil). Two series of tests were performed on soil samples of different relative densities; $D_r = 85\%$ (high density, HD) and 45% (low density, LD) [27].

Vertical static loads of 300 and 100 kN were applied in the HD and LD tests, respectively. The footing was not loaded to failure and thus the bearing capacity could not be determined from the test results. The lateral cyclic testing comprised three phases with different loading schemes. Only Phase III, which involves sinusoidal displacement cycles of increasing amplitude (shown in Fig. 16), is considered in the validation.

All loading phases were conducted in succession with the same experimental setup, i.e. the soil has been loaded above the initial imposed static load before Phase III cyclic loading commenced. The state of the soil could thus be described as partially over-consolidated. Loading was applied to the foundation using an actuator placed at 0.9 and 0.935 m above the foundation in the HD and LD cases, respectively. The actuator was located on the south side and the motion occurred in the north-south direction [27].

The foundation was modeled only in the north-south direction using the proposed assemblage. The footing horizontal force–displacement behavior was modeled using a shear hinge connected in series with an elastic frame member. The moment-rotation behavior of the footing was modeled using a curvature hinge. The tributary length of the curvature hinge was taken as 0.20 m, same as the tributary length of the elastic frame member used with the shear hinge. Table 2 gives the soil properties considered for the HD and LD tests (after [26]).

Perform-3D requires defining the element nonlinear force-deformation behavior using a bilinear or trilinear relation. Thus, to obtain better agreement with the experimental results for the validation process, the moment–curvature relation of the moment hinge and the shear force–shear displacement relation of the shear hinge assembly were defined using trilinear relations. The actual moment–rotation relation of rectangular footings (shown in Fig. 2) was calculated using the soil properties given in Table 2. The corresponding moment–curvature relation of the footing was calculated by dividing the rotation values by the tributary length of the hinge. The required trilinear moment–curvature relation assigned to the curvature hinge was obtained using a trilinear approximation to the calculated moment–curvature relation. A complete description of the approximation procedure can be found in El Ganiany [16].

The trilinear shear force–shear displacement relation of the shear hinge assembly was calculated considering the guidelines shown in Fig. 13. The slope of the elastic branch of the relation represents the elastic horizontal stiffness of the footing, K_H. The horizontal capacity of the footing, F_u, was calculated as the vertical load acting on the footing (300 and 100 kN for the HD and LD

Table 2
Vertical and horizontal stiffness and bearing capacity model parameters for TRISEE experiments (After [26,1]).

	HD Test	LD Test
Vertical response		
Vertical load (kN)	300.00	100.00
Vertical bearing capacity safety factor	5.00	5.00
q_u (kN/m^2)	1500.00	500.00
k_v (kN/m^3)	280,000	100,000
Horizontal response		
K_H (kN/m)	100,000	40,000
F_y (kN)	70.00	22.50

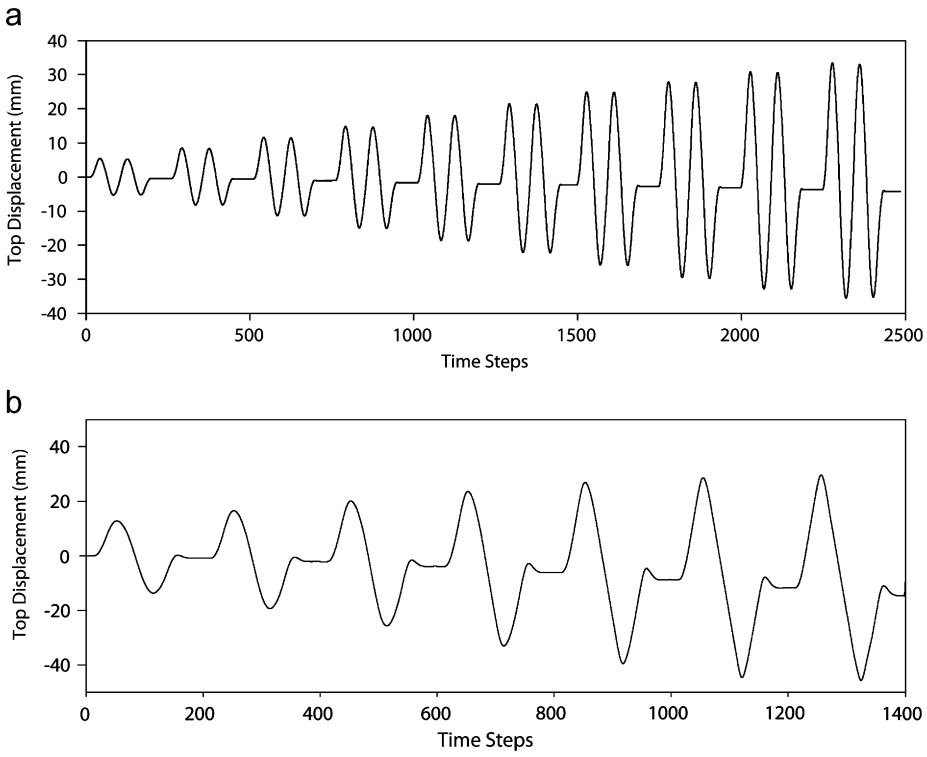

Fig. 16. TRISEE input displacement time histories: (a) HD test; (b) LD test.

tests) multiplied by the friction coefficient between the footing base and soil. A friction coefficient of $0.6\tan(\phi'_{cv})$ was used for both HD and LD tests. This value is slightly smaller than the value of $0.75\tan(\phi'_{cv})$ recommended by FEMA 356 [6] document for concrete–soil interfaces, but it was found to give better fit with the experimental results.

The trilinear shear force–shear displacement relation of the shear hinge assembly also requires the horizontal yield force, F_y, and the shear displacement corresponding to the footing horizontal capacity. The horizontal yield force, F_y, was taken as reported by Allotey [1] for the HD and LD tests. However, the shear displacement corresponding to the footing horizontal capacity was obtained by fitting the experimental horizontal force–displacement hysteresis loops for the HD and LD tests with the hysteresis loops obtained from Perform-3D. A value of 5 and 4 mm for the HD and LD tests, respectively, was found to give a good fit. It should be noted that these shear displacement values were only required for the trilinear representation of the shear force–shear displacement relation used herein in the validation step. However, the bilinear approximation should be sufficient for modeling the footing behavior of real buildings. Hence, the elastic horizontal stiffness of the footing, K_H, and its horizontal capacity, F_u, will be the only parameters required to define the shear force–shear displacement relation of the footing.

3.2. Soil squeeze out phenomenon

An important aspect of moment-rotation behavior of shallow foundations under seismic loading is the so called "soil squeeze out" from beneath the footing edges under rocking action. Knappett et al. [25] have identified this phenomenon from the results of their 1 g shaking table tests on a shallow strip footing model. The dominant failure mechanism was due to rocking action. The foundation soil has yielded beneath the right edge of the footing, while the left edge experienced uplift. The yielded soil zone beneath the right edge of the footing experienced permanent deformation in the form of settlement and "soil squeezing out" from beneath the footing towards the right side. This permanent deformation caused a decrease in the volume of soil beneath the right edge of the footing, which reduced the contact area under the footing in case of moment reversal, thus reducing the moment-rotational stiffness in the next cycle. This explains the S-shape of the hysteretic moment–rotation curves obtained from the experiments.

The same behavior was observed in TRISEE experiment [26]. This behavior depends on the soil relative density as it influences the shape of the failure surface in the foundation soil under a vertically loaded footing.

To account for this phenomenon in the analysis, the moment-rotation stiffness of the footing (or the curvature hinge) should be reduced upon reversal of moment direction. This has been accounted for in Peform-3D model by defining an energy degradation factor, e, for the curvature hinge. This factor is defined as the area of the degraded hysteresis loop divided by the area of the non-degraded loop. Perform-3D uses this factor to adjust the unloading stiffness upon moment reversal. The degraded elastic and hardening stiffness are calculated such that the area of the degraded loop is equal to e times the area of the non-degraded loop. It should be noted that in TRISEE experiment the soil did not experience any stiffness or strength degradation. However, the energy degradation factor has been used to model the reduction in the moment-rotation stiffness of the footing due to the soil squeeze out phenomenon.

The experimental hysteretic moment–rotation curves are fitted to the curves obtained from Perform-3D, yielding values of $e = 0.55$ and 0.8 for the HD and LD tests, respectively. Further experimental data from large scale tests are necessary to verify the validity of these values considering various parameters like footing shape, different soil types and depth of embedment.

3.3. Results and discussion

The proposed model was used to analyze the TRISEE experiments. Figs. 17–20 compare the experimental and numerical hysteretic moment–rotation curves and hysteretic horizontal force–displacement curves for the HD and LD tests. In general, the agreement between the two sets is good, verifying the ability of the proposed approach to simulate shallow foundations behavior. It should be noted that the numerical curves slightly overestimate the hysteretic damping. However, the geometric damping neglected in this approach, would decrease this difference in actual structures.

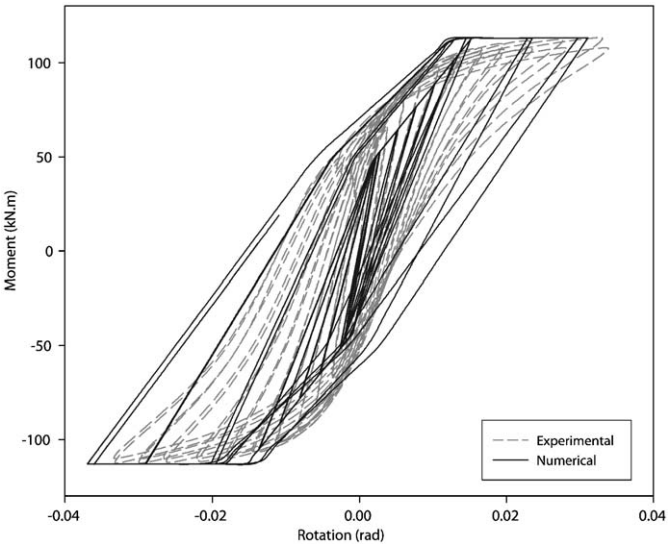

Fig. 17. Comparison of experimental and numerical hysteretic moment–rotation curves for the HD test.

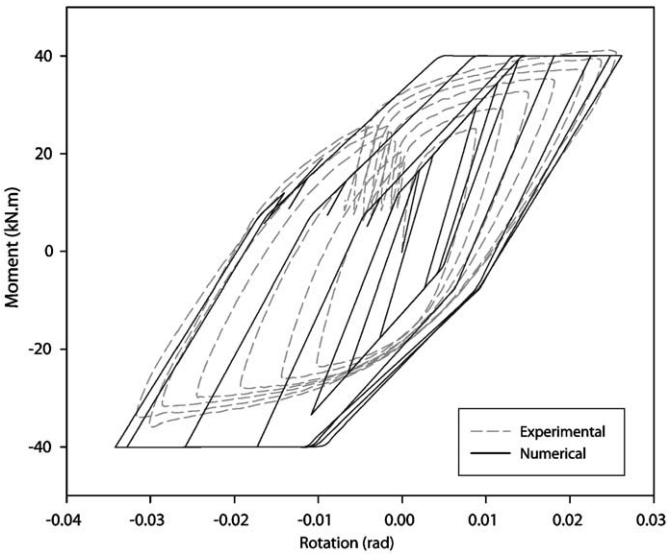

Fig. 18. Comparison of experimental and numerical hysteretic moment–rotation curves for the LD test.

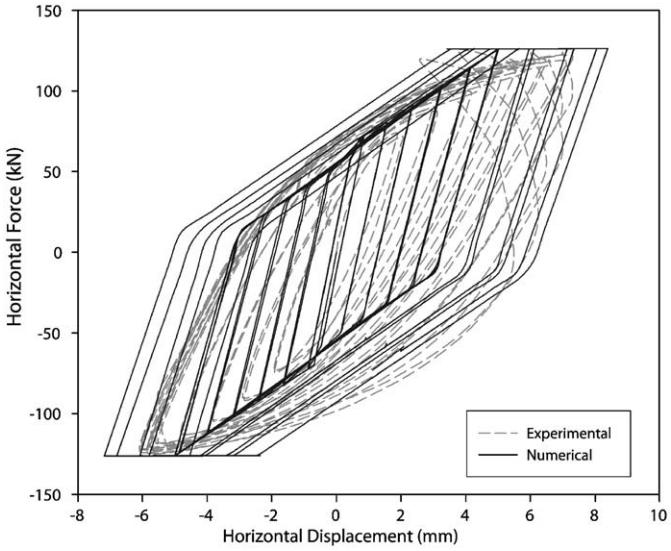

Fig. 19. Comparison of experimental and numerical hysteretic horizontal force–displacement curves for the HD test.

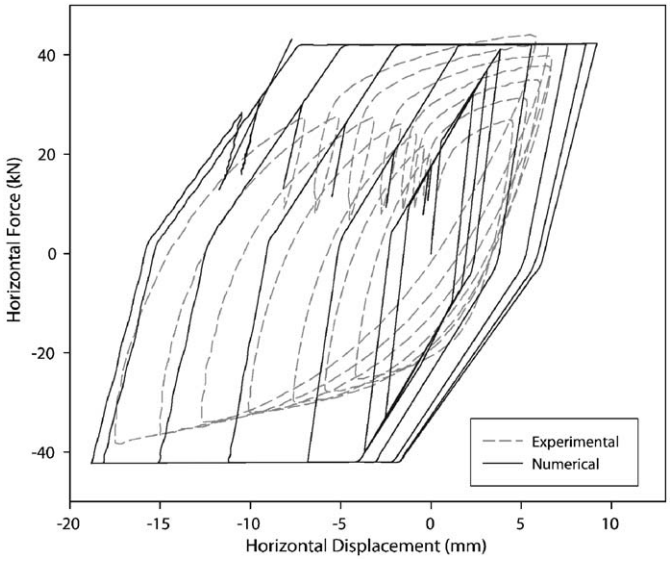

Fig. 20. Comparison of experimental and numerical hysteretic horizontal force–displacement curves for the LD test.

4. Summary and conclusions

This paper presented a new modeling approach based on the BNWF model to simulate the 3D rocking, vertical and horizontal responses of shallow foundations using structural elements that are readily available in the element library of commercially available structural analysis programs. An assemblage of a moment-rotation hinge, shear hinge connected in series with an elastic frame member are attached at the bottom of ground story columns to model the response of the footing under combined action of vertical, horizontal and moment loading.

A bounding surface that defines the interaction between the rocking and vertical capacities of the footing was introduced and its equations have been derived mathematically. A bounding surface that defines interaction between the horizontal capacities of the footing was also established. These bounding surfaces can be incorporated in available structural analysis programs. Simple calculation steps to evaluate the properties of the proposed assemblage of structural elements are also provided.

Two alternative models for analyzing the moment-rotation response of shallow foundations are introduced: moment-rotation hinge and moment-curvature hinge. The moment-rotation hinges are the default moment hinges available in most structural analysis programs. However, the moment-curvature hinges are easier to implement.

The proposed modeling approach was verified using experimental results from large scale model foundations subjected to cyclic loading. The following conclusions may be drawn:

(1) The proposed assemblage of a moment-rotation hinge, shear hinge connected in series with an elastic frame member can simulate the rocking and horizontal responses of shallow foundations under cyclic loading with good accuracy.
(2) It is important to accurately simulate the soil squeeze out phenomenon when analyzing the response of shallow foundations subjected to cyclic rocking action. It affects the amount of hysteretic damping resulting from the moment-rotation response. The effect of this phenomenon can be included in the model by assigning an appropriate energy degradation factor. More comparisons with experimental results are needed to quantify the variation of this factor with different parameters involved in the footing model.

References

[1] Allotey NK. Nonlinear soil–structure interaction in performance based design. Ph.D. Thesis, University of Western Ontario, London, Ontario, Canada, 2006.
[2] Allotey NK, El Naggar MH. An investigation into the Winkler modeling of the cyclic response of rigid footings. Soil Dyn Earthquake Eng 2008;28(1):44–57.
[3] Allotey NK, El Naggar MH. Soil-structure interaction in performance-based design-a review. In: Proceedings of the Predictions, analysis and design in geomechanical applications, proceedings of 11th international conference on computational methods and advances in geomechanics. 2005, p. 595–602.
[4] Allotey NK, El Naggar MH. Analytical moment–rotation curves for rigid foundations based on a Winkler model. Soil Dyn Earthquake Eng 2003;23(5):367–81.
[5] American Society of Civil Engineers. ASCE 41-Seismic rehabilitation of existing buildings, American Society of Civil Engineers, 2006.
[6] American Society of Civil Engineers. FEMA 356-Prestandard and commentary for the seismic rehabilitation of buildings, Federal Emergency Management Agency, Washington, D.C, 2000.
[7] Anderson DL. Effect of foundation rocking on the seismic response of shear walls. Can J Civil Eng 2003;30(2):360–5.
[8] Auvinet G, Mendoza MJ. Comportamiento de diversos tipos de cimentacion en la zone lascustre de la Ciudad de Mexico durante el sismo del 19 septiembre de 1985. in: Proceedings of the symposium-Los Sismos de 1985: casos deMecanica de Suelos. Mexico, 1986, (in Spanish).
[9] Building Seismic Safety Council. FEMA 273/274-NEHRP guidelines for the seismic rehabilitation of buildings, vol. I-guidelines, vol. II-commentary. Federal Emergency Management Agency, Washington, D.C., 1997.
[10] Chaallal O, Ghlamallah N. Seismic response of flexibly supported coupled shear walls. J Struct Eng 1996;122(10):1187–97.
[11] Chen X, Lai Y. Seismic response of bridge piers on elasto-plastic Winkler foundation allowed to uplift. J Sound Vib 2003;266(5):957–65.
[12] Comartin CD, Keaton JR, Grant PW, Martin GR, Power MS. Transitions in seismic analysis and design procedures for buildings and their foundations. Victoria, British Columbia, 1996.
[13] Computers and Structures Inc. Perform-3D—A computer program for nonlinear analysis and performance assessment of 3D structures. 2007a, (4.0.3).
[14] Computers and Structures Inc. Perform-3D-User manuals. 2007b, (4.0.3).
[15] Cremer C, Pecker A, Davenne L. Cyclic macro-element for soil-structure interaction: material and geometrical non-linearities. Int J Numer Anal Methods Geomech 2001;25(13):1257–84.
[16] El Ganainy HM. Seismic performance of buildings with multiple underground stories. M.E.Sc. Thesis, University of Western Ontario, London, Ontario, Canada, 2008.
[17] El-Tawil S, Deierlein GG. Nonlinear analysis of mixed steel-concrete frames. I: element formulation. J Struct Eng 2001;127(6):647–55.
[18] El-Tawil S, Deierlein GG. Nonlinear analysis of mixed steel-concrete frames. II: implementation and verification. J Struct Eng 2001;127(6):656–65.
[19] Filiatrault A, Anderson DL, DeVall RH. Effect of weak foundation on the seismic response of core–wall type buildings. Can J Civil Eng 1992;19(3):530–9.

[20] Gajan S, Thomas JM, Kutter BL. Physical and analytical modeling of cyclic load-deformation behavior of shallow foundations. In: Proceedings of the 57th annual meeting of earthquake engineering research institute. Mexico, 2005.
[21] Gazetas G. SSI issues in two European projects and a recent earthquake. In: Proc, 2nd US-Japan workshop on soil–structure interaction. Tsukuba, Japan, 2001.
[22] Houlsby GT, Cassidy MJ. A plasticity model for the behavior of footings on sand under combined loading. Geotechnique 2002;52(2):117–29.
[23] Housner GW. Behavior of inverted pendulum structures during earthquakes. Seismol Soc Am-Bull 1963;53(2):403–17.
[24] Hutchinson TC, Raychowdhury P, Chang B. Nonlinear structure and foundation response during seismic loading: dual lateral load resisting systems. In: Proceedings of the Eighth US national conference on earthquake engineering. Paper No. 320, San Francisco, California, USA, 2006.
[25] Knappett JA, Haigh SK, Madabhushi SPG. Mechanisms of failure for shallow foundations under earthquake loading. Soil Dyn Earthquake Eng 2006; 26(2–4):91–102.
[26] Negro P, Paolucci R, Pedretti S, Faccioli E. Large scale soil–structure interaction experiments on sand under cyclic load. In: Proceedings of the 12th world conference on earthquake engineering. Paper no. 1191, Auckland, New Zealand, 2000.
[27] Negro P, Verzeletti G, Molina J, Pedretti S, Lo Presti D, Pedroni S. Large scale geotechnical experiments on soil–foundation interaction. Special Publication no. I.98.73, European Commission Joint Research Centre, Ispra, Italy, 1998.
[28] Paolucci R. Simplified evaluation of earthquake-induced permanent displacements of shallow foundations. J Earthquake Eng 1997;1(3):563–79.
[29] Psycharis IN, Jennings PC. Rocking of slender rigid bodies allowed to uplift. Earthquake Eng Struct Dyn 1983;11(1):57–76.
[30] Song Y, Lee D. Improved two-spring model for foundation uplift analysis. Comput Struct 1993;46(5):791–805.
[31] Trifunac MD, Todorovska MI. Reduction of structural damage by nonlinear soil response. J Struct Eng 1999;125(1):89–97.